Stabilizing effect of bedrock uplift on retreat of Thwaites Glacier, Antarctica, at centennial timescales

Book, Cameron
Hoffman, Matthew James
Kachuck, Samuel
Hillebrand, Trevor Ray
Price, Stephen F. Dr
Perego, Mauro
Bassis, Jeremy

To be published in: Earth and Planetary Science Letters

DOI to publisher's version: 10.1016/j.epsl.2022.117798

Earth and Planetary Science Letters 597 (2022) 117798

Contents lists available at ScienceDirect

Earth and Planetary Science Letters

www.elsevier.com/locate/epsl

Stabilizing effect of bedrock uplift on retreat of Thwaites Glacier, Antarctica, at centennial timescales

Cameron Book [a], Matthew J. Hoffman [a,*], Samuel B. Kachuck [b], Trevor R. Hillebrand [a], Stephen F. Price [a], Mauro Perego [c], Jeremy N. Bassis [b]

[a] Fluid Dynamic and Solid Mechanics Group, Los Alamos National Laboratory, Mail Stop B216, Los Alamos, 87544 NM, USA
[b] Climate and Space Sciences and Engineering, University of Michigan, 2455 Hayward St., Ann Arbor, 48109 MI, USA
[c] Center for Computing Research, Sandia National Laboratories, P.O. Box 5800, MS 1320, Albuquerque, 87185 NM, USA

ARTICLE INFO

Article history:
Received 2 June 2022
Received in revised form 25 August 2022
Accepted 27 August 2022
Available online xxxx
Editor: R. Bendick

Keywords:
glaciers
glacial isostatic adjustment
Antarctica
ice-sheet modeling

ABSTRACT

Viscoelastic rebound of the solid Earth upon the removal of ice loads has the potential to inhibit marine ice sheet instability, thereby forestalling ice-sheet retreat and global mean sea-level rise. The timescale over which the solid Earth - ice sheet system responds to changes in ice thickness and bedrock topography places a strong control on the spatiotemporal influence of this negative feedback mechanism. In this study, we assess the impact of solid-earth rheological structure on model projections of the retreat of Thwaites Glacier, West Antarctica, and the concomitant sea-level rise by coupling the dynamic ice sheet model MALI to a regional glacial isostatic adjustment (GIA) model. We test the sensitivity of model projections of ice-sheet retreat and associated sea-level rise across a range of four different solid-earth rheologies, forced by standard ISMIP6 ocean and atmospheric datasets for the RCP8.5 climate scenario. These model parameters are applied to 500-year, coupled ice-sheet - GIA simulations. For the mantle viscosity best supported by observations, the negative GIA feedback leads to a reduction in mass loss that remains above 20% after about a hundred years. Mass-loss reduction peaks at 50% around 2300, which is when a control simulation without GIA experiences its maximum rate of retreat. For a weaker solid-earth rheology that is unlikely but compatible with observational uncertainty, mass loss reduction remains above 50% after 2150. At 2100, mass loss reduction is 10% for the best-fit rheology and 25% for the weakest rheology. At the same time, we estimate that water expulsion from the rebounding solid Earth beneath the ocean near Thwaites Glacier may increase sea-level rise by up to 20% at five centuries. Additionally, the reduction in ice-sheet retreat caused by GIA is substantially reduced under stronger climate forcings, suggesting that the stabilizing feedback of GIA will also be an indirect function of emissions scenario. We hypothesize that feedbacks between the solid Earth - ice sheet system are controlled by a competition between the spatial extent and timescale of bedrock uplift relative to the rate of grounded ice retreat away from the region of most rapid unloading. Although uncertainty in solid-earth rheology leads to large uncertainty in future sea-level rise contribution from Thwaites Glacier, under all plausible parameters the GIA effects are too large to be ignored for future projections of Thwaites Glacier of more than a century.

1. Introduction

The West Antarctic Ice Sheet has the capacity to raise global mean sea level (GMSL) by approximately three meters by delivering ice to the oceans through the dynamics of its outlet glaciers (Feldmann and Levermann, 2015; Martin et al., 2019). In particular, Thwaites Glacier (see inset in Fig. 1a) has been speeding up (by 50–100 m yr^{-1}) and increasing in ice mass loss (by 10–15 Gt yr^{-1}) over the past decade (Scambos et al., 2017). Estimates indicate that it is currently contributing approximately 0.1 mm yr^{-1} to sea level (Scambos et al., 2017) and, under complete collapse, has the potential to contribute 65 cm to GMSL from the ice within its current catchment, while inducing additional retreat in the neighboring catchments of West Antarctica (Martin et al., 2019). It has recently been suggested that collapse of Thwaites is imminent and perhaps ongoing (Joughin et al., 2014; Waibel et al., 2018). As such, an understanding of the timescale and dynamics of its evolution is critical for forecasting GMSL changes.

* Corresponding author.
E-mail address: mhoffman@lanl.gov (M.J. Hoffman).

https://doi.org/10.1016/j.epsl.2022.117798

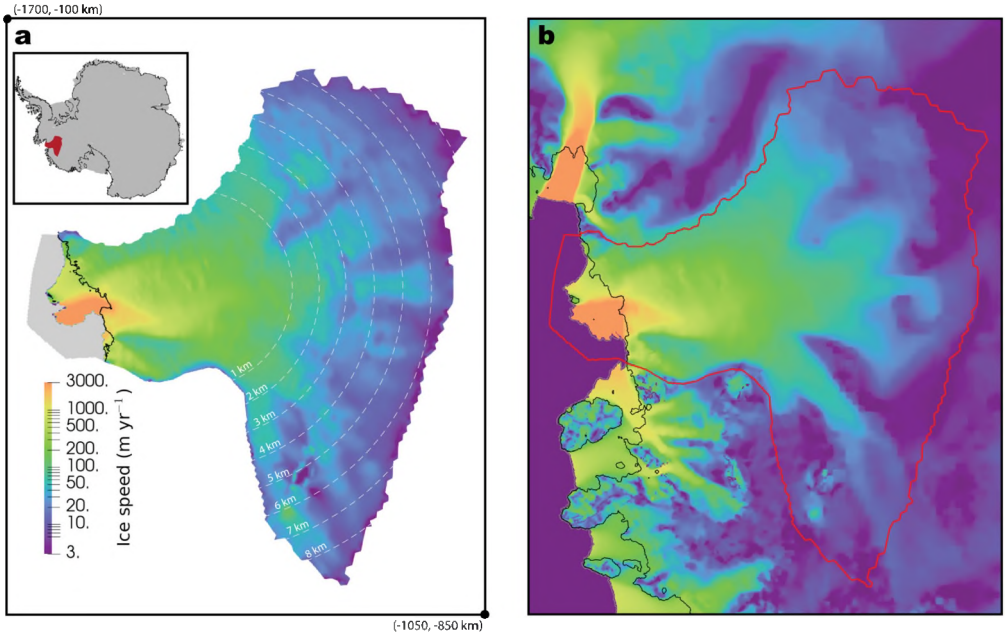

Fig. 1. Thwaites Glacier domain for ice-sheet model. a) Modeled ice surface speed from model initial condition. Black line indicates grounding-line position. Dashed white contours indicate cell spacing of the mesh. Gray area is part of the model mesh but is ice-free ocean. The two coordinate points in the corners of the map identify the model domain location in a Polar Stereographic projection with true scale at 71°S and WGS84 ellipsoid. Inset map shows location of Thwaites Glacier in Antarctica. b) Observed ice surface speed from satellite-derived measurements of Rignot et al. (2014). Red line indicates boundary of the ice-sheet model computational domain. The GIA computational domain is a rectangle three times larger than the extent shown here. (For interpretation of the colors in the figure(s), the reader is referred to the web version of this article.)

Accompanying the redistribution of ice and sea water during evolution of glaciers such as Thwaites are the concomitant perturbations to the Earth's crust, rotation, and gravitational potential field through the processes of glacial isostatic adjustment (GIA) (Whitehouse et al., 2019). Of these GIA effects, the deformation of Earth's solid surface (hereafter called lithosphere) to changing ice loads is of primary importance to ice-sheet dynamics. It has been demonstrated that the response of the lithosphere to surface unloading via ice-sheet retreat has the potential to forestall further retreat (Gomez et al., 2010, 2015; Barletta et al., 2018; Larour et al., 2019) by limiting the effectiveness of the marine ice-sheet instability (MISI; Schoof, 2007). Whereas the gravitational and rotational changes induced by glacier mass changes can be significant for regional sea-level changes around the Earth (Gomez et al., 2010), the deformation of the lithosphere is the dominant GIA mechanism impacting local glacier evolution and stabilization of MISI, particularly on centennial time scales (Gomez et al., 2015; Larour et al., 2019; Kachuck et al., 2020; Coulon et al., 2021).

MISI theory describes a positive feedback mechanism that operates by means of a non-linear relationship between grounding line flux and the ice thickness at the grounding line (where grounded ice goes afloat due to buoyancy). As the grounding line retreats across topography deepening toward the ice sheet interior, ice thickness at the grounding line increases, causing greater grounding-line flux, flux divergence, and dynamic thinning. This thinning in turn leads to local flotation and further landward retreat of the grounding line. Viscoelastic uplift of bedrock beneath the retreating ice sheet serves to regionally decrease sea level, thereby moving the grounding line downglacier, potentially slowing, stalling, or even re-advancing the ice sheet (Gomez et al., 2015; Kachuck et al., 2020).

The rate at which the surface rebounds upon removal of a surface load depends primarily on the viscosity of the mantle, and the wavelength and magnitude of the deformation has been shown to be depend strongly on lithosphere thickness (Nield et al., 2018). Consequently, mantle viscosity and lithosphere thickness can directly influence the potential of the solid Earth to mitigate ice-sheet retreat. Although in many Antarctic GIA studies, laterally-invariant, global/continent-wide average magnitudes of both mantle viscosity and lithosphere thickness are invoked, several recent seismic tomography studies have revealed appreciable lateral variations in these rheological properties across Antarctica, and evidence of particularly low mantle viscosity and lithosphere thickness in West Antarctica (Lloyd et al., 2020).

Thwaites Glacier is located within a region of West Antarctica that has recently been posited to overlay an area of markedly low mantle viscosity ($\sim$ 1e18–1e19 Pa s; Barletta et al., 2018), which is two to three orders of magnitude lower than the global average of $\sim$ 1e21 Pa s. Thwaites Glacier has displayed significant retreat in recent years and is situated over a reverse-sloped bed relatively devoid of bedrock ridges and lateral constraints that could inhibit retreat (Cornford et al., 2015; Joughin et al., 2014; Scambos et al., 2017). As such, it is potentially susceptible to MISI dynamics; however, its position above a region of low viscosity mantle could counteract the positive feedback. Although several regional modeling studies have focused on the evolution of Thwaites Glacier (Seroussi et al., 2017; Waibel et al., 2018; Yu et al., 2018, 2019; Hoffman et al., 2019), most have not addressed the effects of viscoelastic rebound of the lithosphere on its evolution. Similarly, while there have been many Antarctic-wide studies investigating the impacts of GIA at millennial timescales (Konrad et al., 2015; Gomez et al., 2015; Pollard et al., 2017; Coulon et al., 2021), there has yet to be a study targeting the effects of low mantle viscosity on Thwaites Glacier over the coming centuries. Larour et al. (2019) considered only the elastic uplift of deformation in the region and reported that localized elastic uplift could substantially slow the retreat of Thwaites Glacier. Kachuck et al. (2020), however, indicated that viscoelastic effects dominate elastic effects and that viscoelastic uplift of the lithosphere could reduce mass loss at neighboring Pine Island Glacier by up to 30% over 150 years. Given these results, assessing the full impact of GIA on the future evolution of Thwaites Glacier remains an unresolved yet important problem.

In this study we investigate the impact of GIA on the future evolution of Thwaites Glacier over 500 years using the MPAS-Albany Land Ice (MALI) ice-sheet model (Hoffman et al., 2018) coupled to the planar, viscoelastic GIA model, giapy (Kachuck, 2017). Consistent with other GIA studies of West Antarctica, we find substantial reductions in mass loss when the low viscosities inferred for the region are used, with elastic effects insignificant. The strength of the GIA feedback is sensitive to the choice of mantle viscosity, which is poorly constrained, leading to large uncertainty in sea-level contribution from Thwaites Glacier. The GIA feedback is also sensitive to the external climate forcing imposed on the glacier and the associated grounding line retreat rate. Results show that GIA effects on the evolution of Thwaites Glacier should not be ignored for the range of solid-earth rheology parameter values estimated for this region.

2. Methods

2.1. Ice-sheet model description

We use the MPAS-Albany Land Ice (MALI) model to simulate the evolution of Thwaites Glacier. MALI is a thermomechanically coupled, higher order ice-sheet model using a mixture of finite element and finite volume methods (Hoffman et al., 2018). MALI solves the first-order, three-dimensional approximation to the nonlinear Stokes equations for ice velocity (also known as the "Blatter-Pattyn" model; Blatter, 1995; Pattyn, 2003) using Nye's generalization of Glen's flow law as the constitutive relation. The velocity solver uses the finite element method on an unstructured mesh (Tezaur et al., 2015). In this study we use a linear viscous basal friction law as in a previous MALI study of Thwaites Glacier (Hoffman et al., 2019). Although a semi-plastic basal friction law may be more appropriate for this region (Gillet-Chaulet et al., 2016), our initial experiments with such a law indicated that results were highly sensitive to assumptions about effective pressure near the grounding line. Other work has shown that model projections of Amundsen Sea sector mass change can be complicated by the choice of basal friction law (Nias et al., 2018). Because this study aims to examine the sensitivity of mass loss due to ice dynamics coupled with GIA, we retained the simpler linear basal friction law and avoid the additional complications introduced by multiple sliding laws. Evolution of ice geometry and tracers is handled through an explicit first-order horizontal advection scheme with vertical remapping. Evolution of ice temperature is treated using operator splitting of vertical diffusion and horizontal advection.

2.1.1. Thwaites Glacier model domain

For the application of MALI to Thwaites Glacier, we use a variable resolution, regional, Voronoi mesh that has 1 km cell spacing in the fast flowing region of Thwaites Glacier, including upglacier through the entirety of the main trunk of the glacier, and then coarsening to 8 km resolution at the inland ice divide (Fig. 1). The mesh has 75500 horizontal grid cells and 10 vertical terrain following levels that increase in resolution at depth. The cell spacing is identical to that used by Hoffman et al. (2019, see Fig. 1a), however we have updated the ice geometry and initial condition. In this study, ice thickness and bed elevation are interpolated from BedMachine Antarctica Version 2 (Morlighem et al., 2020). At the lateral boundaries of the regional domain we apply specified velocity Dirichlet boundary conditions using the present-day observed velocity field from Mouginot et al. (2017). However, for thickness evolution we apply no-flux boundary conditions normal to the domain boundary to prevent leakage of mass outside the current catchment boundary. This approach prevents the possibility of divide migration, but has a minimal impact on lateral buttressing for a glacier as wide as Thwaites Glacier (Martin et al., 2019). Calving physics are not explicitly modeled; the calving front is not allowed to advance beyond the initial position but can retreat if thinning from submarine melting reduces ice thickness to zero. MALI uses an adaptive time stepping algorithm set by the advective Courant-Friedrich-Levy (CFL) condition. For the mesh resolution and ice velocities in these simulations, the time step typically ranges between 0.07-0.4 years, but varies substantially over time as the velocity field evolves.

The spatial distribution of the linear basal friction coefficient and a steady-state ice temperature field used as the initial condition for ice temperature are determined simultaneously through a partial differential equation constrained optimization problem (Perego et al., 2014). In this approach, the adjoint capability of MALI is used to solve an inverse problem minimizing the misfit of ice surface velocity relative to observations (from Mouginot et al., 2017), subject to regularization and satisfying the first-order momentum balance (velocity solver) and steady state thermodynamics (enthalpy solver). The thermodynamics uses a Dirichlet boundary condition for surface temperature from RACMO2.3 mean-annual air temperature (Lenaerts et al., 2012) and assumes a thawed bed subject to the geothermal heat flux of Shapiro and Ritzwoller (2004) such that the bed temperature is enforced to be at the melting point using a penalty method. In the forward simulations, ice temperature evolves, but the basal friction coefficient field is held fixed.

2.1.2. Climate forcing

Surface mass balance and ice-shelf basal melting follow the ISMIP6-Antarctica protocol (Seroussi et al., 2020; Jourdain et al., 2020). This protocol applies surface mass balance anomalies from a climate model added to a baseline historical surface mass balance field, which we take from RACMO2.3p1 (van den Broeke, 2019). For ice-shelf basal melting, we use the ISMIP6 non-local parameterization (Jourdain et al., 2020) that is proportional to the product of the ocean thermal forcing (difference between ocean temperature and local freezing temperature) averaged across an ice-shelf cavity and the local thermal forcing at each grid cell. Our primary ensemble follows ISMIP6-Antarctica experiment 5, which uses climate forcing from NorESM1-M under the RCP8.5 greenhouse gas emissions scenario and a medium sensitivity of ice-shelf melting to ocean thermal forcing. We selected this forcing configuration because it was the primary projection used by the ISMIP6 model intercomparison assessment (Seroussi et al., 2020). It is in the top three climate models for reproducing historical conditions around Antarctica, and it projects moderate warming of the Amundsen Sea by the end of the century (Barthel et al., 2020). By choosing an RCP8.5 greenhouse gas scenario, we are able to explore ice-sheet/GIA interactions under a plausible but more extreme forcing, particularly given that the forcing projection ends at 2100 and thus likely underestimates changes in climate in later centuries. We perform an additional set of simulations following ISMIP6-Antarctica experiment 13, which uses the same climate model forcing, but a higher ocean melt sensitivity that was specifically tuned for the grounding-line region of Pine Island Glacier, which neighbors Thwaites Glacier.

2.2. GIA model

We compute vertical land motion using the flat-earth module of the open-source, Python package *giapy* (Kachuck, 2017). Its solution method is based on an approach developed by Bueler et al. (2007) that invokes the fast Fourier transform (FFT) to efficiently calculate the viscoelastic response of a planar solid to an arbitrary surface load. To determine the magnitude of transient, vertical bedrock uplift, the model calculates a bedrock uplift rate

Table 1
Simulations conducted and solid-earth rheological parameters used. CTRL is a control run with the GIA model disabled. TYP represents typical rheology globally, but uses a viscosity that is too large for West Antarctica. BEST2 are the parameter values identified as "Best2" used by Barletta et al. (2018) and Kachuck et al. (2020). VLV and VLV-THIN use the lowest mantle viscosity that is compatible with geophysical observations, with two different possible lithosphere thicknesses. h is thickness of the upper mantle layer, h_e is lithosphere thickness, and D is the flexural rigidity of the lithosphere. The low viscosity runs, VLV and VLV-THIN, have a single mantle layer, so h is not applicable. The Maxwell time is an approximate value based on the upper mantle viscosity and shear modulus.

	CTRL	TYP	BEST2	VLV	VLV-THIN
Shallow upper mantle viscosity (Pa s)	-	2×10^{20}	4×10^{18}	1×10^{18}	1×10^{18}
Lower mantle viscosity (Pa s)	-	4×10^{21}	2×10^{19}	1×10^{18}	1×10^{18}
h (km)	-	670	200	-	-
h_e (km)	-	60	60	60	25
D (N m)	-	13×10^{23}	13×10^{23}	13×10^{23}	1×10^{23}
Maxwell time (yr)	-	238.4	4.8	1.2	1.2

at each time step based upon an approach to isostasy associated with the change in surface mass loading calculated from isostatic equilibrium and the cumulative uplift from all previous time steps.

The GIA model consists of a three-layered earth: a thin, elastic lithosphere and two mantle layers, delineated by viscosity. The upper mantle layer has a specified thickness and viscosity, while the lower layer is treated as a viscous half-space with a specified viscosity. The elastic layer is represented in the model by a single parameter, the flexural rigidity, D. Although D varies laterally across Antarctica (Coulon et al., 2021), and recent studies have highlighted how the elastic response of the lithosphere depends on loading frequency (Lau et al., 2021; Nield et al., 2018), we assume D to be spatiotemporally invariant over our regional domain. The flexural rigidity may be related to the elastic thickness of the lithosphere, h_e, through the following relationship for a thin-plate under flexure,

$$D = \frac{E h_e^3}{12(1-\nu^2)}, \tag{1}$$

where $E = \frac{\mu(3\lambda+2\mu)}{\lambda+\mu}$ is Young's modulus and $\nu = \frac{\lambda}{2(\lambda+\mu)}$ is Poisson's ratio. We utilize a Lame's first parameter of $\lambda = 34.2667$ GPa, a shear modulus of $\mu = 26.6$ GPa from the uppermost layer of PREM, and a uniform density of 3313 kg m^{-3} from the first mantle layer of PREM (Dziewonski and Anderson, 1981).

Although we choose to omit variations with depth in these parameters, the responses of this simplified model to loading captures that of a layered, viscoelastic mantle (see a discussion of the differences in the Supplementary Material of Kachuck et al., 2020). Additionally, in our calculation of the Maxwell timescales for each modeling scenario, we make the assumption that a single, unique relaxation timescale may be determined using average values for both upper mantle viscosity and shear modulus. In reality, there exists a spectrum of relaxation times, since the timescale depends upon the wavelength of the surface load (Wu and Peltier, 1982), as well as on the upper mantle viscosity and shear modulus, both of which vary with depth and loading timescale (Lau et al., 2021). Therefore, while there is inherent uncertainty in our calculated Maxwell timescales related to the choice of these parameters, the timescales fall within the range of previously estimated values (Whitehouse et al., 2019; Coulon et al., 2021).

Changes in the surface mass load occur as both the mass of the ice changes, as described in the previous section, and as vertical land motion modifies ocean bathymetry and changes the mass of overlying ocean water. Our model assumes constant sea surface geoid height, and thus does not account for changes in ocean loading due to near-field or far-field gravitational changes. We take the load and surface to be in isostatic equilibrium at the onset of the simulation (year 2015), an assumption that results in an underestimate of uplift but was shown to have a small impact for neighboring Pine Island Glacier (Kachuck et al., 2020). Further, as indicated in Whitehouse et al. (2019), due to the short Maxwell times estimated for West Antarctica, the solid Earth response is relatively insensitive to the prior loading history beyond a decade, which is reflected in the low viscosity scenarios of our modeling. Though our model does not include self-gravitation, sea-level interactions, and rotational changes, a key feature of this model is the wavelength-dependence of the relaxation time, which captures the short-wavelength (< 1000 km) behavior of a spherically symmetric, self-gravitational, non-rotating viscoelastic body (Kachuck and Cathles, 2019). For further details regarding model set-up, see Kachuck et al. (2020).

Here, *giapy* is run using a 1 km resolution rectangular mesh that extends over a region about three times as extensive as the MALI regional Thwaites Glacier domain. Additionally, the spatial extent is expanded by an additional factor of three for the FFT calculation to ensure long wavelength deformation is resolved, to enforce mass conservation in mantle deformation, and to avoid aliasing within the domain. Because the solution is sensitive to domain extent due to the long wavelengths of deformation, we selected the domain extent through sensitivity tests by applying extreme mass load changes to increasingly larger domain sizes until calculated uplift was converged to $< 2\%$. Similarly, sensitivity tests of GIA model time step were conducted to select a time step of 0.1 years as being sufficiently short to not affect model accuracy.

2.3. Solid-Earth parameters and experimental design

We considered a suite of four realistic solid-earth rheologies, focusing on two key parameters: mantle viscosity and lithosphere thickness. Values for these solid-earth properties are based upon various recent Antarctic geodetic campaigns and GIA modeling studies (e.g. Nield et al., 2014; Barletta et al., 2018; Simms et al., 2012; Kachuck et al., 2020), and can be found in Table 1. Although we implement static values for mantle viscosity and lithosphere thickness in each of our runs, it is important to note that these properties are not necessarily constant or independent of dynamic, deformational processes within the solid earth. Indeed, it has been shown that effective/apparent viscosity, lithosphere thickness, Maxwell timescales, and rheological properties in general can exhibit dependence on both stress magnitude and loading frequency (Blank et al., 2021; Lau et al., 2021). Such power-law (stress-dependent) and transient rheological processes may impact the response timescales of ice-sheet/solid-earth feedback systems, particularly in events of rapid unloading wherein mantle viscosity appears to decrease and lithosphere thickness increases due to the rate and magnitude of melt-induced load changes, thereby influencing uplift rates and ice mass loss estimates. While we note the potential impact of these processes on our projections as well as the importance of exploring these mechanisms in future work, we do not consider them here.

Our high viscosity bound (based on Ivins et al., 2013), TYP, has an upper mantle viscosity of 2×10^{20} Pa s for the top 670 km of the mantle, lower mantle viscosity of 4×10^{21} Pa s, and 60 km thick lithosphere, typical of most of the Earth and appropriate for East

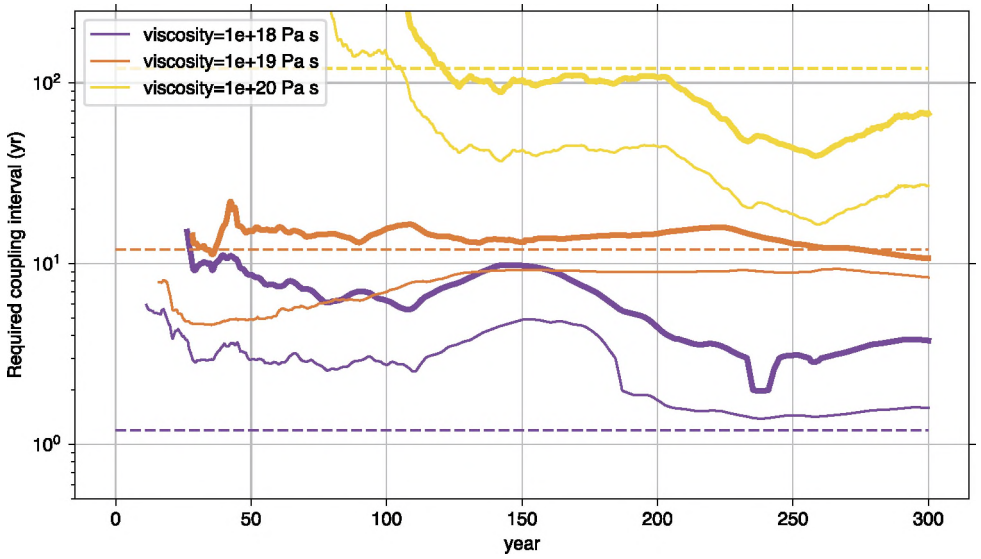

Fig. 2. Required coupling interval between ice-sheet and GIA models to maintain low error in simulated glacier mass loss. Thick line represents 5% error and thin line 2% error. Dashed line represents approximate Maxwell time calculated as the ratio of the upper mantle viscosity and shear modulus (taken here as 26.6 GPa from the uppermost layer of PREM, Dziewonski and Anderson, 1981). Results are using a preliminary 4 km MALI mesh run for 300 years with constant climate forcing. Analyis is performed for a high viscosity solid-earth rheology (yellow), an intermediate viscosity rheology (orange), and a low viscosity rheology (purple) (similar to TYP, BEST2, and VLV-THIN, respectively).

Antarctica. The intermediate rheology, BEST2, is based on "Best2" from the GPS-constrained GIA modeling of glacial retreat in the Amundsen Sea Embayment by Barletta et al. (2018), and consists of a shallow upper mantle viscosity of 4×10^{18} Pa s for the top 200 km of the mantle, lower mantle viscosity of 2×10^{19} Pa s, and lithosphere thickness of 60 km. In addition, we performed two lower-bound runs with very low viscosity, VLV and VLV-THIN, with uniform mantle viscosity of 1×10^{18} Pa s and lithosphere thicknesses of 60 km and 25 km, respectively. The VLV parameters are meant to represent the lowest, locally estimated bound on mantle strength in the region, and are based on Barletta et al. (2018), Nield et al. (2014), and (Kachuck et al., 2020). The choice in VLV mantle viscosity 1×10^{18} Pa s reflects the best-fit viscosity found in the GPS-constrained GIA modeling of the Antarctic Peninsula (viscoelastic model using Palmer Station and LARISSA network cGPS) by Nield et al. (2014), and the lowest shallow-upper mantle viscosity considered by Barletta et al. (2018, Fig. S5) that was able to describe uplift patterns in the Amundsen Sea Embayment. This value is intended to indicate a reasonable estimate of a best-case scenario (with respect to ice mass conservation) based on physical estimates, not necessarily a likely possibility. Note, however, that a slightly higher or lower choice in VLV mantle viscosity would impact the resultant uplift patterns in our modeling. It should also be noted that lithosphere thickness values used correspond well to those estimated for the Amundsen Sea Embayment in the GIA modeling of Blank et al. (2021). Finally, we also conduct a reference control run, CTRL, that has the GIA model disabled.

All simulations are integrated for 500 model years, starting nominally in 2015 and following the ISMIP6-Antarctica protocol (Seroussi et al., 2020). The ISMIP6 climate forcing only extends 85 years to 2100, and we hold climate forcing fixed at its final values after that (similar to Chambers et al., 2021). All configurations shown in Table 1 are simulated for the ISMIP6-Antarctica medium ocean sensitivity parameter (ISMIP6-Antarctica experiment 5). Additionally, we conduct CTRL and VLV-THIN experiments using the high ocean sensitivity parameter (ISMIP6-Antarctica experiment 13), as described above. We refer to these as HM-CTRL and HM-VLV-THIN.

2.4. Model coupling and performance

MALI is coupled to `giapy` using offline data files, where each model is run for a predetermined coupling interval, writes coupling fields to a data file, and terminates, after which the other model is executed for the same interval. MALI communicates the change in the combined load of ice and ocean water across the MALI domain, and `giapy` communicates the bedrock uplift rate. We found that using bedrock uplift rate instead of bedrock elevation resulted in higher accuracy by allowing MALI to spread bedrock changes evenly across its own time steps (order 0.01–0.1 years) and by avoiding degradation of the bedrock topography field through repeated interpolations. In contrast, the ice-mass load used by giapy remains constant over each coupling interval for simplicity. The coupling fields are interpolated between each model's grid using bilinear interpolation.

We performed sensitivity tests on the coupling interval between the two models using a preliminary 4–14 km resolution MALI domain run for 300 years for characteristic mantle rheologies. We defined a required coupling interval as that which permits $< 2\%$ error in cumulative glacier mass loss relative to a coupling interval of 1 year. We found for the highest mantle viscosity used, a coupling interval of multiple decades was sufficient, whereas for the weakest solid-earth rheology, the minimum coupling interval was generally less than 10 years and reached a minimum of less than 2 years for part of the simulation (Fig. 2). Noticing that these results are similar in magnitude to the Maxwell timescale (ratio of dynamic viscosity and elastic shear modulus; Table 1), we suggest this as a rule-of-thumb for offline coupling interval. However we caution that the time-dependence of the minimum coupling intervals shown in Fig. 2 indicate that factors such as the rate of mass loss can also contribute to the timescale of ice-sheet/solid-earth interactions. Based on these considerations and our computational resources, we apply a 1 year coupling interval to ensure errors from the coupling frequency are negligible.

All simulations are conducted on the Cori supercomputer's Knights Landing architecture at the U.S. Department of Energy's National Energy Research Supercomputing Center (NERSC). MALI is run using 340 processors and giapy is a serial code running on 1 processor. The throughput of the combined model is primarily

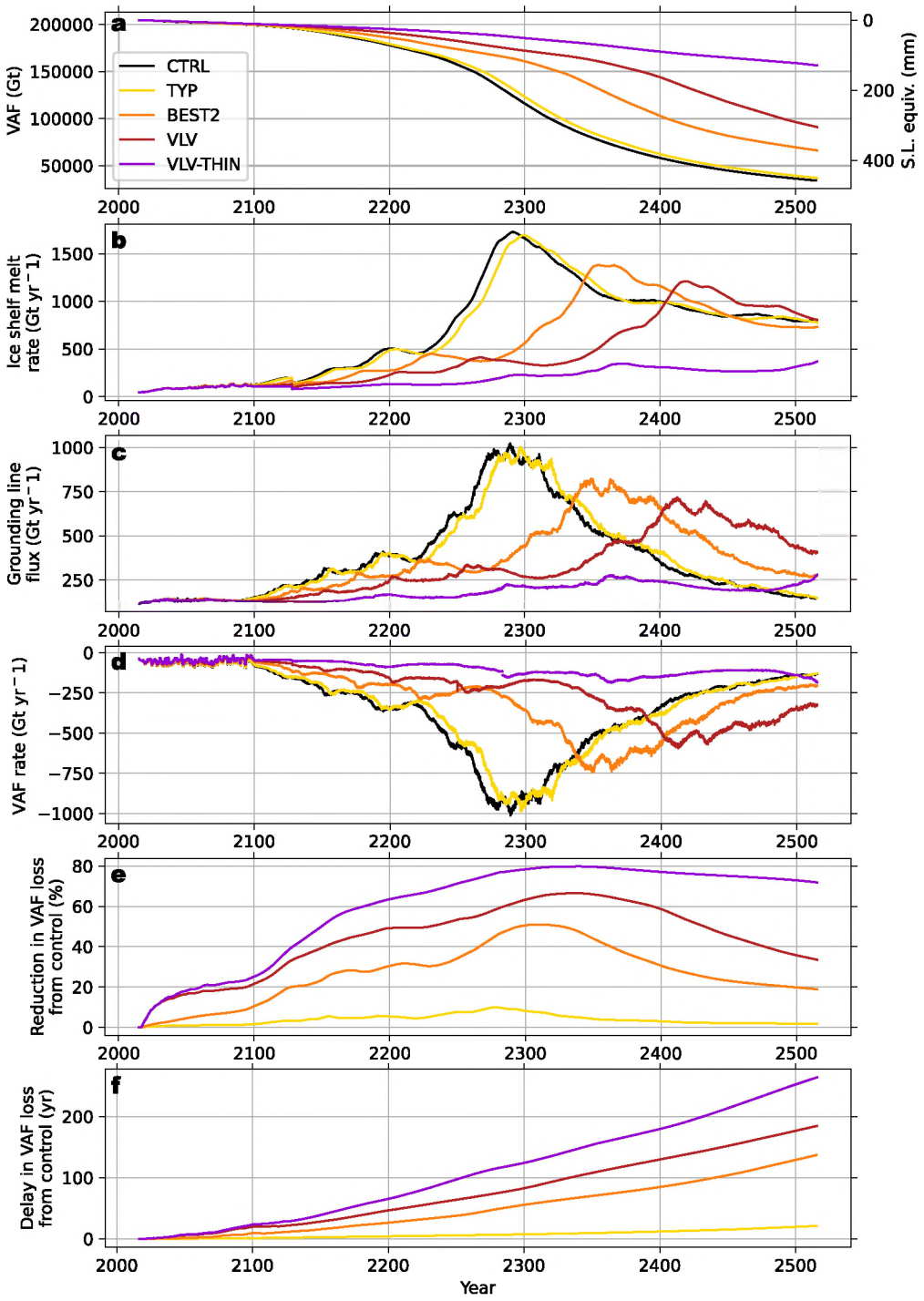

Fig. 3. Time series of results from each model run. a) Volume above flotation. b) Ice shelf basal melt rate. c) Flux across the grounding line. d) Rate of change of volume above flotation. e) Reduction in mass loss relative to control run. f) Delay in mass loss relative to control run.

controlled by MALI simulation and varied between about 2.5 and 7.0 simulated years per wall-clock hour, depending on the CFL-restricted MALI time step. Total computing cost for each 500-year simulation was about 60 thousand CPU-hours.

3. Results

3.1. Control run

In the CTRL experiment, with fixed bedrock, the grounding-line flux in the first 5 years of the simulation (2015–2020) ranges between 113 and 124 $Gt\,yr^{-1}$ (Fig. 3c), which is comparable to measured grounding line flux of 115–132 $Gt\,yr^{-1}$ in the 2006–2010 time period (Mouginot et al., 2014). The mass loss rate, calculated as change in volume above flotation, increases from about 40 to 75 $Gt\,yr^{-1}$ over the first five years (Fig. 3d). It remains between 50 and 100 $Gt\,yr^{-1}$ for the first century, after which it increases to about 250 $Gt\,yr^{-1}$ at 2150 as the grounding line retreats into deeper bed topography (Fig. 4). Mass loss continues to increase until about 2290 at which point it reaches about 1000 $Gt\,yr^{-1}$ (Fig. 3d) as the grounding line traverses the deepest topographic basin (Fig. 4b). After this, mass loss rate gradually reduces through the end of the simulation at 500 years, at which point the catch-

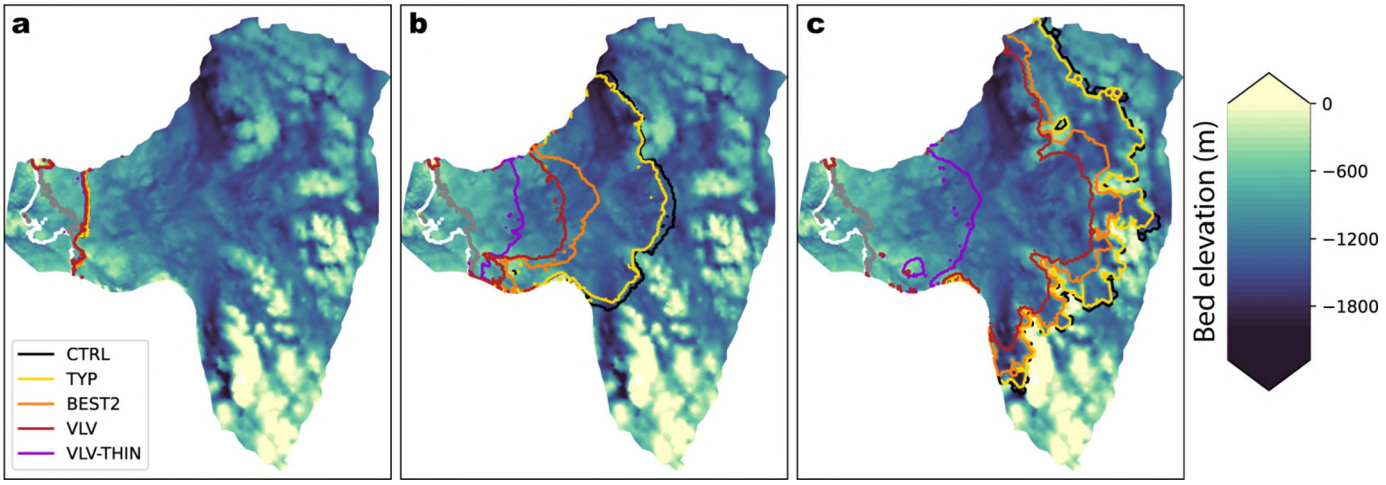

Fig. 4. Grounding-line positions at different times for each run, overlying a map of the initial bed elevation from Morlighem et al. (2020). a) At 2100. b) At 2300. c) At 2515. Initial grounding line position is shown in gray, and ice-shelf calving front position is shown in white.

ment is largely deglaciated (Figs. 3d, 4c). The cumulative barystatic contribution to sea-level rise at 2515 is 458 mm (Fig. 3a). As stated in the Methods, climate forcing is held fixed after 2100, so this is likely an underestimate of the rate of retreat in later centuries. Changes in ice-shelf melt flux (Fig. 3b) over the first 85 years are driven by an increase in ocean thermal forcing. The much larger increases in ice-shelf melt flux later in the simulation are associated with a rapid increase in ice-shelf area as the grounding line retreats but the calving front position remains fixed. Some retreat of the ice-shelf calving front occurs in the final half of the simulation as basal melting outpaces the replenishment of ice from advection and surface accumulation.

3.2. Effects of GIA

3.2.1. Influence of solid-Earth rheology

When the coupling to the GIA model is included, all runs exhibit reduced glacier mass loss relative to the control run. Mass-loss reduction gradually increases over the first few centuries, peaking in each simulation around 2300 when the control run experiences its most rapid rate of mass loss (Fig. 7a, e). The solid-earth rheology for typical mantle conditions (TYP) exhibits 8% less mass loss at 2300 than the control run. There is a substantially larger impact with the best-fit solid-earth rheology for the region; BEST2 leads to a 51% reduction in sea-level contribution at 2300. For the extreme low viscosity rheologies, mass loss reduction at 2300 is far greater. VLV yields a 64% reduction, and VLV-THIN a 79% reduction (Fig. 3e). The reduction in sea-level contribution is more modest earlier in the run; at 2100 reductions are 2%, 10%, 22%, and 25% for TYP, BEST2, VLV, and VLV-THIN, respectively.

In all cases, the reduction in sea-level contribution is caused by delayed retreat of the grounding line, with the weaker solid-earth rheology simulations taking longer for the grounding line to retreat to and through the large overdeepened basin in the center of the catchment (Fig. 4). Thus, reductions in mass loss correspond to delays in glacier evolution relative to the control run without GIA, and these delays grow progressively over time (Fig. 3f). At the end of the simulations in 2515, this delay is 137 years for BEST2; the volume of Thwaites Glacier in BEST2 at 2515 corresponds to the volume of the control run in 2378. For VLV-THIN, the delay is 263 years. Mass loss delay at the end of the first century are 10 years for BEST2 and 27 years for VLV-THIN.

Peak uplift generally occurs near the grounding line (Fig. 5), though spatial patterns of bed uplift are a function of both mass loss and solid-earth rheology. For the very low viscosity configurations that have a rapid viscoelastic response, peak uplift is near the grounding line (Fig. 5c-d), while for the slower adjusting mantle of BEST2, peak uplift occurs further downglacier of the grounding line (Fig. 5a-b). Increases in grounding line flux and associated mass loss rates occur later in the weaker rheology runs and exhibit lower peak rates (Fig. 3a-c). Though VLV and VLV-THIN use the same mantle viscosity, the thinner lithosphere of VLV-THIN results in more localized uplift that increases bed elevation at the grounding line for a given glacier mass loss and therefore is more effective at slowing grounding line retreat.

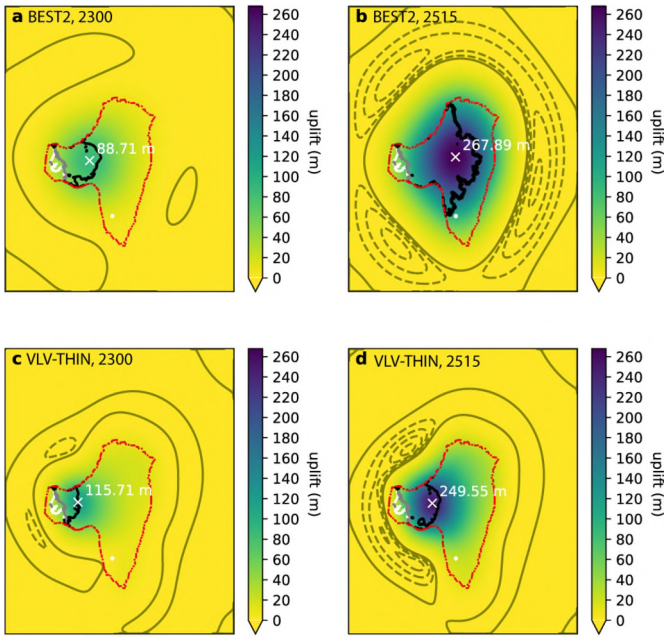

Fig. 5. Maps of cumulative uplift. a) BEST2 run at 2300. b) BEST2 run at 2515. c) VLV-THIN run at 2300. d) VLV-THIN run at 2515. Colorbar range is truncated at zero, and the zero contour is marked by solid olive lines. Areas of subsidence are contoured with intervals of 1 m in dashed olive lines. The location and magnitude of maximum uplift is marked by a white x and label. White line is calving-front position, gray line is initial grounding-line position, and black line is grounding-line position at given time. Results are shown on the giapy domain, and the red dashed line indicates the boundary of the MALI domain.

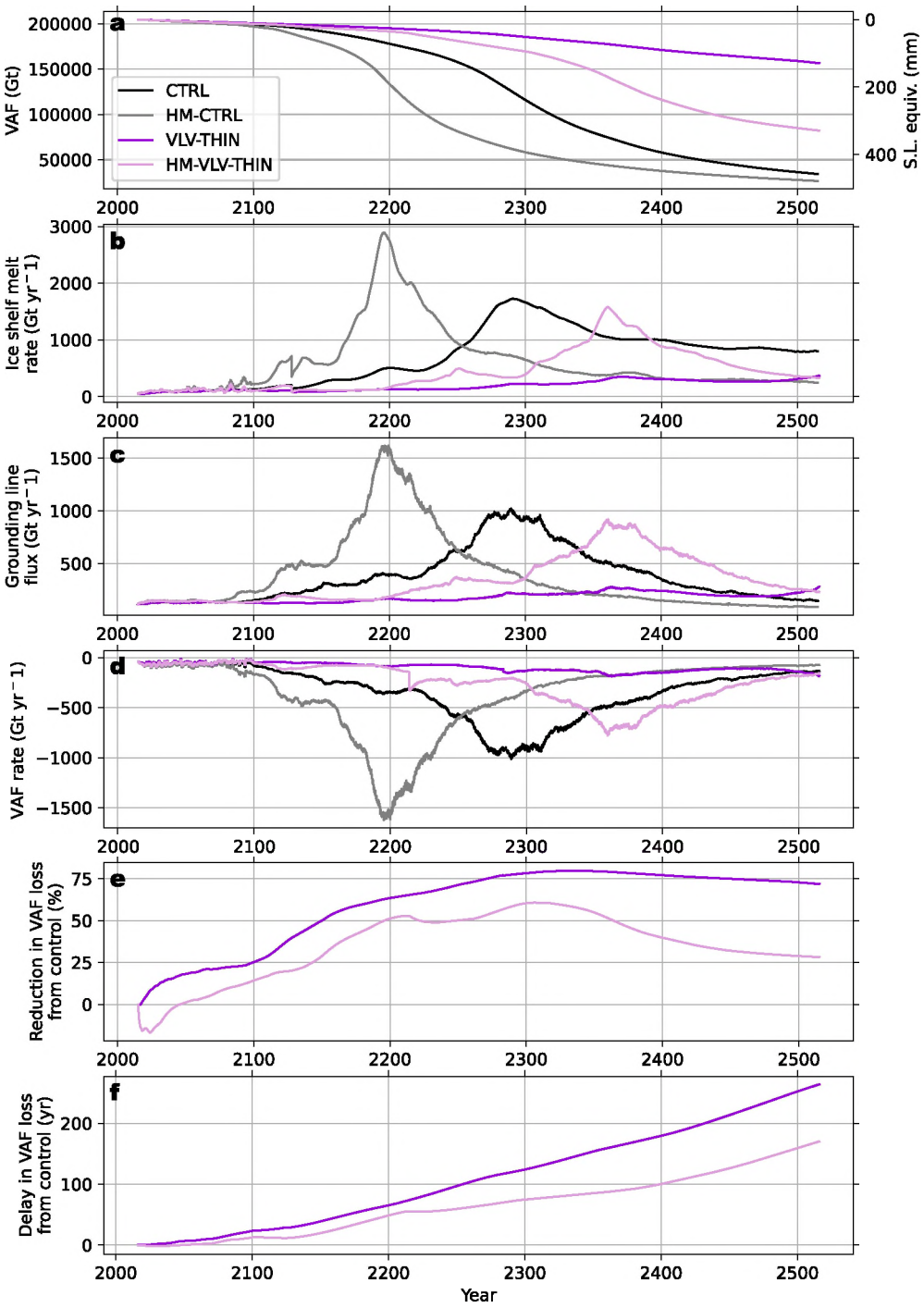

Fig. 6. Same as Fig. 3 but comparing VLV-THIN for standard and high melt (HM) ocean melt sensitivity.

3.3. *Effects of varying melt forcings*

To investigate the impact of climate forcing on the GIA feedback, we compare the results of VLV-THIN and HM-VLV-THIN, the corresponding configuration with higher ocean melt sensitivity. The HM-CTRL simulation has slightly greater cumulative mass loss through 2515 than the CTRL simulation — 479 mm GMSL equivalent versus 458 mm (Fig. 6a). However, in both simulations the Thwaites catchment is largely deglaciated after 500 years, obscuring the fact the HM-CTRL simulation retreats much more quickly. In HM-CTRL, the inflection to rapid mass loss occurs about 100 years earlier around 2175, consistent with the higher ice-shelf melt rates (Fig. 6a, b). As seen for the VLV-THIN simulation, HM-VLV-THIN also exhibits substantially reduced retreat relative to a fixed bedrock. However, with the higher melt rate forcing, the impact of GIA is reduced. When using the standard melt forcing, inclusion of the low viscosity GIA model led to a 72% reduction in mass loss at 2515, whereas for the high melt forcing, the reduction is 31%. With the more rapid grounding line retreat resulting from the more rapid melting, grounded ice retreats before viscoelastic uplift has sufficient time to make a large impact on bed elevation. The more localized spatial extent of uplift due to the thin lithosphere used for these runs augments this effect.

4. Discussion

4.1. Comparison to similar studies without GIA

The CTRL run without GIA yields similar results to previous modeling studies of Thwaites Glacier with fixed bedrock. The high melt control run, HM-CTRL, is also similar to previous studies in the first century, but exhibits an earlier transition to rapid mass loss and higher peak mass loss rates than most previous studies. In the first 50 years, CTRL yields 8.5 mm sea-level rise and HM-CTRL 10.2 mm. Mass loss in the CTRL run is less than in our previous Thwaites Glacier study (10.1 mm sea-level equivalent at 50 years; Hoffman et al., 2019), consistent with our improved initial condition having a slightly lower initial grounding line flux (113 vs. 125 $\mathrm{Gt\,yr^{-1}}$). Our two studies also use different ice-shelf basal melt parameterizations, but they yield comparable melt rates over the first century ($\sim$15–20 $\mathrm{m\,yr^{-1}}$). Mass loss over the first 50 years in both the standard and high melt control runs is also similar but smaller than the mass loss of 12.1–13.3 mm sea-level equivalent after 50 years reported by Seroussi et al. (2017).

After the first century, CTRL simulates 18.3 mm sea-level equivalent, whereas HM-CTRL gives 28.0 mm, compared to 25.9 mm from our previous study (Hoffman et al., 2019). These values are within the range of the previous ensembles by Yu et al. (2018, 14–42 mm SLE for a range of ice dynamics and melting scenarios) and Yu et al. (2019, 12–30+ mm SLE for a range of calving and melting scenarios). For the configuration most similar to ours (momentum balance approximation, basal friction law, melt scenario) from Yu et al. (2018), their study projects 15–22 mm SLE, and for Yu et al. (2019) (fixed calving front), 12 mm SLE after 100 years. Our CTRL simulation is also similar to the 20.1 mm SLE after 100 years reported by Cornford et al. (2015, reported as 75 $\mathrm{Gt\,yr^{-1}}$) for Thwaites Glacier.

The general similarity of CTRL to previous studies holds for the second century. The mean loss rate of volume above flotation over the second century in CTRL is 250 $\mathrm{Gt\,yr^{-1}}$, which is larger than the 212 $\mathrm{Gt\,yr^{-1}}$ from our previous study (Hoffman et al., 2019). This can be explained by the fact that melt rates remained at present day rates in Hoffman et al. (2019), but evolve through 2100 according to the ISMIP6 protocol in the current study, leading to higher ice-shelf melt rates and reduced buttressing. Over this time period, Cornford et al. (2015) reports volume above flotation loss of 320 $\mathrm{Gt\,yr^{-1}}$, and Joughin et al. (2014) shows rates of 150–200 $\mathrm{Gt\,yr^{-1}}$, with one ensemble member substantially larger. In contrast, our HM-CTRL simulation averages mass loss of 813 $\mathrm{Gt\,yr^{-1}}$ during the second century, as the grounding line retreats into the deepest bathymetry of the basin much earlier (Fig. 4).

At the longest time scales, previous modeling studies all indicate a period of rapid mass loss that initiates as the grounding line retreats into the overdeepened topographic basin in the catchment and which subsequently ends as the majority of the catchment becomes deglaciated. Waibel et al. (2018) analyzed the initiation of MISI during this period and found it to occur around 260 years into their simulation. Using the corresponding inflection in total mass and grounding line position as a guide, Martin et al. (2019) show a similar time using the same model as Waibel et al. (2018), as does our previous study with MALI (Hoffman et al., 2019). Joughin et al. (2014) used a threshold of 1 $\mathrm{mm\,yr^{-1}}$, which represents a similar point in glacier evolution to the unstable state identified by Waibel et al. (2018), and for which they found their ensemble reached anywhere from year 212 to beyond 1000 years, depending on scenario. In our current simulations, the phase of rapid mass loss occurs in year 215 for CTRL and year 145 for HM-CTRL. The more rapid transition to apparent MISI in our simulations can be explained by the fact that the other studies use ice-shelf melt forcing for present day conditions, whereas our simulations described here have ocean thermal forcing that increases through 2100 following the ISMIP6 protocol.

Based on these comparisons, we consider our two control runs to be representative of moderate and more extreme forced retreat of Thwaites Glacier. It should be emphasized that although ocean thermal forcing evolves in our simulations, the climate model data driving the forcing ends after the first 85 years, so both melt configurations represent a conservative amount of ice-shelf melting in later centuries (potentially strongly so) should ocean thermal driving continue to increase after 2100. With these considerations, our simulations with the two melt configurations capture a wide range of potential interactions between ice-sheet evolution and solid-earth response.

4.2. Comparison to similar studies with GIA

This study adds to a large body of previous work investigating the impact of GIA on future evolution of the Antarctic Ice Sheet covering a wide range of timescales and model complexity. The majority of these have focused on timescales of a millennium or longer and therefore used relatively coarse resolution (8–40 km) and lower-fidelity ice-sheet models (Konrad et al., 2015; Gomez et al., 2015; Pollard et al., 2017; Coulon et al., 2021; Chambers et al., 2021). For studies using higher mantle viscosities similar to our TYP case, significant impacts from GIA were typically not seen for 1000 years or more (Konrad et al., 2015; Gomez et al., 2015; Pollard et al., 2017; Coulon et al., 2021), consistent with negligible impacts of GIA over the 500 years of our TYP simulation. Previous studies are in agreement that lower mantle viscosity leads to delays in glacier retreat at millennial time scales, but it was not until the findings of extremely low mantle viscosity by Barletta et al. (2018) that ice sheet modelers considered mantle viscosities below 10^{19} Pa s in Antarctica.

Only a few studies thus far have considered the impacts of very low mantle viscosity. DeConto et al. (2021) considered the same rheology as our BEST2 parameters in a global sea-level model coupled to a 10 km resolution ice-sheet model of the entire Antarctic Ice Sheet for a range of RCP forcings. They see only small differences when including GIA over the first couple hundred years, similar to our BEST2 results and modest impacts at 250 years (approximately 10–25% reduction in sea-level contribution). Similar to our results using high melt sensitivity forcing, they find that GIA impacts are much smaller under extreme climate forcing. Because they simulated the entire ice sheet and with a uniform solid-earth rheology for both West and East Antarctica, it is not clear how their results for Thwaites Glacier, specifically, compare to ours. Considering an Elastic Lithosphere-Relaxing Aesthenosphere model with equivalent mantle viscosities ranging between $10^{18} - 10^{21}$ coupled to an 8 km resolution ice-sheet model, Coulon et al. (2021) found large decreases in mass loss of West Antarctica due to GIA at centennial and millennial timescales at the lowest equivalent viscosity values, consistent with our results at 500 years. They also find that more extreme climate forcing reduces the impact of GIA.

Kachuck et al. (2020) presented a similar study to ours. They use the same GIA model and parameters, a different high resolution ice-sheet model, and different climate forcing applied to neighboring Pine Island Glacier for 150 years. At 150 years, they found mass loss reduction of a few percent for the TYP solid-earth parameters, a 12% reduction for BEST2, and 29% for VLVTHIN. Our reductions at that time are substantially larger: 4.7%, 27.9%, and 56.4%, respectively (Fig. 3e). Although it is difficult to directly compare the two studies, we hypothesize that the steeper overdeepening and wider catchment geometry of Thwaites Glacier is the primary reason for the larger impact of GIA we find here; bed uplift can provide a greater stabilizing force to a basin subject

to more rapid rates of mass loss. Our Thwaites Glacier CTRL run exhibits a 4.5 times increase in mass loss rate between 100 and 150 years into the simulation, as the grounding line retreats into a large overdeepened basin (Fig. 4). The Pine Island Glacier control run of Kachuck et al. (2020) exhibits a ∼1.5 times increase over the corresponding period.

4.3. Factors controlling feedbacks between glacier retreat and bedrock uplift

Kachuck et al. (2020) showed that effects of elastic uplift are negligible for low viscosity solid-earth rheologies (BEST2, VLV). Following the analysis of Kachuck et al. (2020), we conducted additional runs with the instantaneous displacement of the elastic lithosphere disabled in the GIA model, such that only the viscous displacement modulated by the flexural rigidity of the lithosphere response is active. In those simulations we see an approximate 2% reduction on the impact of GIA, consistent with their results. Larour et al. (2019) presented results from an ice-sheet model with 1 km resolution coupled to a global GIA model that included elastic uplift only but refined to 1-km resolution in Antarctica. They reported a 0.12 m reduction in Thwaites Glacier's contribution to sea level after 2350 (equivalent to a 15-30% reduction in SLR or a 23 year delay in glacier retreat). They argue that elastic uplift is important at high (∼1 km) spatial resolution. Here, despite using 1 km resolution in both our ice-sheet and GIA models, we are unable to reproduce their results showing a significant impact of elastic uplift on glacier evolution. Our TYP simulation, with a millennial scale viscoelastic timescale, is comparable to an elastic-only configuration over the 500-year timescale simulated, yet the mass loss reduction in that run never exceeds a few percent. Our finding of the negligible impact of elastic uplift for realistic ice-sheet mass changes agrees with Kachuck et al. (2020) and Wan et al. (2021).

In contrast, we find that lithosphere thickness and the associated flexural rigidity of the lithosphere has an important effect on the GIA-glacier feedback. Our run with the lowest viscosity and thinnest lithosphere (25 km), VLV-THIN, reduced Thwaites' contribution to sea-level rise at 2515 by 80%, when compared to the control run. However, the same mantle viscosity with a thicker 60 km lithosphere (VLV) yields a substantially smaller stabilizing effect. Indeed, the change from a 60 km thick lithosphere (VLV) to 25 km (LV-THIN) has a greater impact than reducing mantle viscosity by more than a factor of 4 (BEST2 to VLV) (Fig. 3a). This is because the thinner lithosphere concentrates uplift near the grounding line where ice is thinning most rapidly, leading to larger local uplift and grounding line stabilization (Fig. 4) for a given ice mass loss. This highlights lithosphere thickness as a critical uncertain parameter that needs to be better constrained in addition to mantle viscosity to reduce uncertainty in future projections of mass loss from West Antarctica. Konrad et al. (2015) also showed that a thinner lithosphere can provide stabilization of the West Antarctic Ice Sheet when it would otherwise collapse for the same mantle viscosity but a thicker lithosphere. Kachuck et al. (2020) similarly showed that lithosphere thickness can be as important as mantle viscosity in slowing retreat of Pine Island Glacier.

To better understand the mechanism by which GIA stabilizes grounding line retreat, we compare glacier conditions between different simulations for a common grounded area, which we use as a proxy for grounding line position (Fig. 7). We find two mechanisms that delay grounding-line retreat. The first is the expected decrease in grounding-line flux at a given grounding-line position for simulations that experience higher bed uplift (Fig. 7c). Because ice thickness at the grounding line is thinner if the bed is shallower (mean grounded ice thickness shown as a proxy in Fig. 7d) and MISI occurs because the grounding-line flux increases nonlinearly with ice thickness at the grounding line (Schoof, 2007), a shallower bed will lead to slower retreat, all else being equal. The second factor we see is that ice-shelf basal melting is decreased for a given grounding-line position when the bed is shallower (Fig. 7b). This occurs because the ice shelf is necessarily thinner when the bed is shallower (Fig. 7e), and ocean thermal forcing, and therefore melt, tends to decrease at shallower ocean depths (Jourdain et al., 2020). In the absence of GIA, relatively higher melt rates for a given grounding-line position lead to relatively greater ice-shelf thinning and reduced ice-shelf buttressing that in turn contributes to more rapid grounding-line retreat. Although the ocean temperature distribution is prescribed in our configurations based on climate model output that does not consider bedrock changes, reduction of melt rates at shallower ocean depths is a robust qualitative feature expected as a result of typical ocean stratification (Asay-Davis et al., 2017; Jourdain et al., 2020; Hoffman et al., 2019). The impact of GIA-driven bathymetric uplift on ocean-driven melting of ice shelves is a topic that deserves further investigation.

4.3.1. Ocean water displacement from submarine uplift

Because the solid-earth response to glacier mass changes can also modify the bathymetry of the neighboring ocean, particularly for marine ice sheets, it is important to also consider impacts on GMSL due to ocean water expulsion from submarine crustal uplift (Goelzer et al., 2020; Pan et al., 2021). Because the viscous component of the displacement is considered incompressible without sources or sinks, viscous subsidence and uplift must average to zero over the Earth. Though a global, spherical sea-level model is necessary to accurately calculate the net effect of near-field submarine uplift and far-field submarine subsidence, we can approximate an upper bound on ocean expulsion in our regional, planar GIA model by calculating the near-field submarine uplift. Because the grounding-line position at neighboring glaciers is unknown in our regional ice-sheet model domain, we make the assumption of a contiguous grounding-line position within the larger GIA model domain to the east (Pine Island Glacier) and west (Pope/Smith/Kohler glaciers). This provides an estimate of what regions of the larger GIA model domain are ocean-based at each time.

Our estimates of maximum possible ocean water expulsion at 2515 range from 11 mm GMSL equivalent for TYP to 66 mm for both BEST2 and VLV, while VLV-THIN experiences 17 mm (dashed lines in Fig. 8). The large magnitude of ocean displacement occurs for different reasons for BEST2 and VLV. The large uplift in BEST2 is due to a substantially larger glacier mass loss than VLV, whereas rapid uplift in VLV is due to the lower viscosity that leads to a more rapid viscoelastic adjustment time scale for a given mass loss. The uplift from VLV-THIN is much lower than VLV despite the same mantle viscosity, because VLV-THIN experiences much less overall mass loss than VLV. Thus, the amount of uplift over the timescales considered here are a strong function of both the change in surface load and the rate at which the solid earth can adjust to the load change.

Near-field ocean displacement could add as much as 13–20% to the barystatic contribution to GMSL rise for BEST2, VLV, and VLV-THIN (shaded regions in Fig. 8). The actual value is likely smaller, because far-field submarine subsidence will offset some of this volume change. However, a significant fraction of far-field subsidence will occur in land-based or ice-sheet-based regions where it would not offset the ocean displacement calculations presented here. Our upper bound estimates here indicate that the reduction in ice-sheet mass loss due to low viscosity solid-earth uplift may be partially offset by increased sea-level rise from ocean expulsion. More detailed calculations with a global, spherical sea-level model are necessary to further constrain the magnitude of this effect. Using a global sea-level model with gravitational effects, Pan et al. (2021) estimate ocean expulsion would increase GMSL rise by 18%

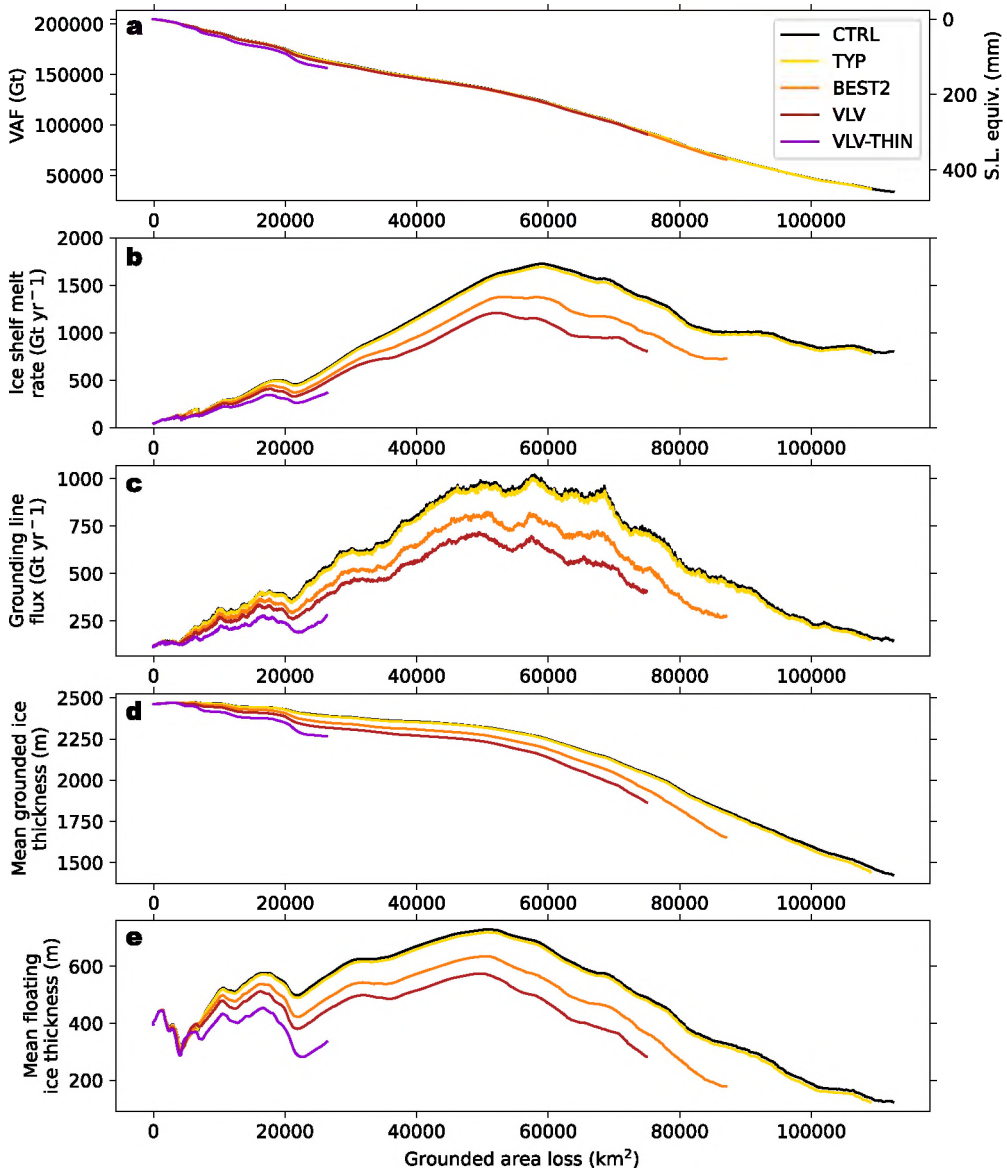

Fig. 7. Results from each model run plotted as a function of loss in grounded area from initial extent, a proxy for grounding-line retreat. a) Volume above floatation. b) Ice-shelf basal melt rate. c) Flux across the grounding line. d) Mean grounded ice thickness. e) Mean floating ice thickness.

from a collapse of West Antarctica over the next century, which is comparable with the relative impact we find with our simpler estimate here. The potential impact of GIA on ocean displacement is much smaller for TYP, where it adds at most 3% to the barystatic contribution (Fig. 8).

4.4. Model limitations and further work

As discussed above, the strong sensitivity of the glacier response to mantle viscosity and lithosphere thickness means that a more precise specification of the solid-earth rheology in West Antarctica is critical for improving projections of ice-sheet evolution and sea-level rise. Specifically, more nuanced characterization and implementation of lithosphere and mantle dynamics and properties are needed, which should entail further integration of frequency-dependent and stress-dependent rheological processes (e.g., creep, relaxation), as well as improved quantification of mantle pre-stresses, structure, temperature, and composition. At the same time, there is considerable lateral variation in solid-earth properties in Antarctica (Ivins et al., 2021; Blank et al., 2021; Barletta et al., 2018; Nield et al., 2018), and three-dimensional GIA models are required to represent these variations and their impact over larger spatial scales (Gomez et al., 2018). We also do not consider the potential impact of ongoing GIA from previous glacier mass loss, but previous studies have shown these effects are likely small for the mantle viscosities and ice mass loss history of West Antarctica, where the viscous response can exceed the elastic response and viscous relaxation occurs rapidly under secular ice mass loss (Whitehouse et al., 2019; Nield et al., 2014; Kachuck et al., 2020). Although the GIA model employed here allows us to calculate uplift at high spatial resolution for relatively small computational expense, our methodology ignores the gravitational and rotational components of GIA and regional sea level. We also ignore far-field sea-level forcing from mass changes of the Greenland Ice Sheet and global mountain glaciers, as well as steric sea-level changes. Previous studies have shown these effects to be small relative to local bedrock deformation over centennial timescales (Konrad et al., 2015; Gomez et al., 2015; Pollard et al., 2017; Larour et al., 2019; Kachuck et al., 2020; Coulon et al., 2021), justifying neglecting them from our study.

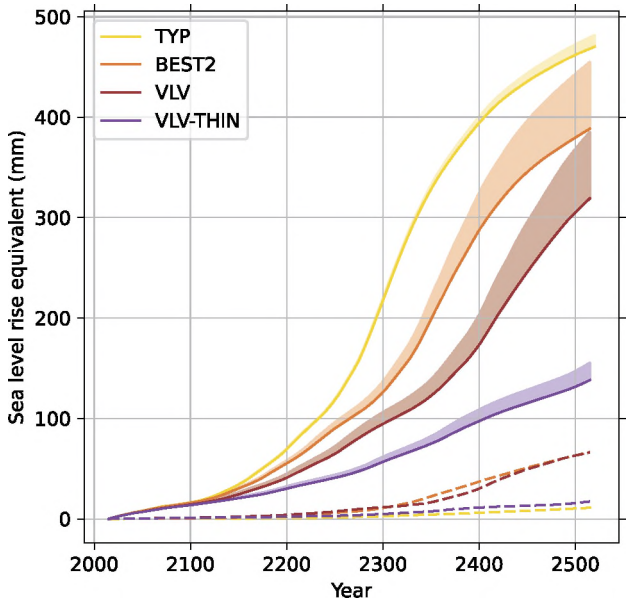

Fig. 8. Effects of submarine uplift on ocean water displacement. Dashed lines show change in ocean basin volume due to submarine uplift, expressed as global mean sea level equivalent. This is an upper bound because it only considers near-field submarine uplift and ignores far-field submarine subsidence. Solid lines show barystatic contribution from Thwaites Glacier mass loss to global mean sea level rise. These are the same curves as Fig. 3a. The shaded regions show the range of total contribution to GMSL rise, considering both barystatic and ocean expulsion processes (dashed plus solid curves).

On the ice-sheet model side of the problem, our configuration ignores a number of important glacier processes, including ice-shelf processes related to damage, calving, and hydrofracture, as well as changes in basal friction driven by subglacial hydrology. Additionally, a semi-plastic basal friction law may be more realistic for this region (Gillet-Chaulet et al., 2016; Nias et al., 2018), which would result in a more widespread pattern of speedup and mass loss (Gillet-Chaulet et al., 2016) and therefore impact the spatial pattern of GIA response. The impact of glacier bed rheology on ice-sheet/GIA interactions deserves further study. Finally, our use of a regional model domain with fixed catchment boundaries prevents the possibility of divide migration, a limitation common to most regional studies (Joughin et al., 2014; Waibel et al., 2018; Yu et al., 2018, 2019). Although these processes are likely to alter glacier evolution and projections of sea-level contribution, they are not expected to be directly modified by GIA, so we consider the differences between our simulations with and without GIA to be generally valid. The climate forcing used in this study suffers from considering only one climate model scenario and by being held constant after 2100. Due to the sensitivity of GIA feedbacks to climate forcing, this is an area that requires further improvement to reduce uncertainty in West Antarctic glacier projections.

5. Conclusions

Our application of a high resolution ice-sheet model of Thwaites Glacier coupled to high-resolution regional GIA model demonstrates that observationally-constrained low mantle viscosity and thin lithosphere can dramatically reduce glacier retreat and sea-level contribution at centennial timescales. This effect is very sensitive to both solid-earth rheological parameters and climate forcing, leading to substantial uncertainty in future sea-level changes. For the mantle viscosity best supported by observations, the stabilizing effect from GIA remains above 20% after about a hundred years and peaks at 50% around 2300, while rheologies at the extreme end of observational constraints yield mass-loss reduction that remain above 50% after a little more than a century. However, the stabilizing effect of GIA substantially declines with stronger climate forcing, because in those scenarios there is not sufficient time for significant uplift before grounded ice retreats. Consequently, the stabilizing effects of GIA are also functions of future climate forcing and thus are not guaranteed to significantly ameliorate future climate impacts from Antarctica. Furthermore, the impact of GIA is relatively small over the coming two centuries, even with the weakest plausible solid-earth rheology. The impact of ocean water displacement from bedrock uplift beneath the ocean adjacent to the glacier also may partially offset the reduction in sea level associated with low viscosity mantle uplift by up to 16%. Future modeling studies projecting evolution of West Antarctica on timescales greater than about a century should include GIA effects, as they substantially modify glacier evolution at longer timescales.

Disclaimer

This paper describes objective technical results and analysis. Any subjective views or opinions that might be expressed in the paper do not necessarily represent the views of the U.S. Department of Energy or the United States Government.

Sandia National Laboratories is a multimission laboratory managed and operated by National Technology and Engineering Solutions of Sandia, LLC, a wholly owned subsidiary of Honeywell International, Inc., for the U.S. Department of Energy's Office of Science under contract DE-NA-0003525.

CRediT authorship contribution statement

Cameron Book: Conceptualization, Formal analysis, Investigation, Methodology, Software, Visualization, Writing – original draft. **Matthew J. Hoffman:** Conceptualization, Formal analysis, Funding acquisition, Investigation, Methodology, Software, Supervision, Validation, Visualization, Writing – original draft. **Samuel B. Kachuck:** Conceptualization, Methodology, Software, Writing – original draft. **Trevor R. Hillebrand:** Data curation, Investigation, Resources, Validation, Writing – review & editing. **Stephen F. Price:** Conceptualization, Funding acquisition, Project administration, Resources, Writing – review & editing. **Mauro Perego:** Investigation, Software, Writing – review & editing. **Jeremy N. Bassis:** Conceptualization, Funding acquisition, Project administration, Writing – review & editing.

Declaration of competing interest

The authors declare that they have no known competing financial interests or personal relationships that could have appeared to influence the work reported in this paper.

Data availability

Model code, model simulation output, and analysis scripts are archived at Zenodo at https://doi.org/10.5281/zenodo.6607706 and https://doi.org/10.5281/zenodo.6607081.

Acknowledgements

This work was supported by the Scientific Discovery through Advanced Computing (SciDAC) program, funded by the US Department of Energy (DOE), Office of Science, Advanced Scientific Computing Research and Biological and Environmental Research programs. This work was also supported by the DOE Office of Science Early Career Research program. Simulations were performed on machines at the National Energy Research Scientific Computing Center, a U.S. Department of Energy Office of Science User

Facility located at Lawrence Berkeley National Laboratory, operated under Contract No. DE-AC02-05CH11231 using NERSC awards ERCAP0016816 and ERCAP0020130. We also used computing resources at the Los Alamos National Laboratory Institutional Computing Program, which is supported by the U.S. Department of Energy National Nuclear Security Administration under Contract DE-AC52-06NA25396. This work is also from the DOMINOS project, a component of the International Thwaites Glacier Collaboration (ITGC). Support from National Science Foundation (NSF: Grant 1738896) and Natural Environment Research Council (NERC: Grant NE/S006605/1). Logistics provided by NSF-U.S. Antarctic Program and NERC-British Antarctic Survey. ITGC Contribution No. ITGC-077.

References

Asay-Davis, X.S., Jourdain, N.C., Nakayama, Y., 2017. Developments in simulating and parameterizing interactions between the Southern Ocean and the Antarctic ice sheet. Curr. Clim. Change Rep. 3, 316–329. https://doi.org/10.1007/s40641-017-0071-0.

Barletta, V.R., Bevis, M., Smith, B.E., Wilson, T., Brown, A., Bordoni, A., Willis, M., Khan, S.A., Rovira-Navarro, M., Dalziel, I., Smalley, R., Kendrick, E., Konfal, S., Caccamise, D.J., Aster, R.C., Nyblade, A., Wiens, D.A., 2018. Observed rapid bedrock uplift in Amundsen Sea Embayment promotes ice-sheet stability. Science 360, 1335–1339. https://doi.org/10.1126/science.aao1447.

Barthel, A., Agosta, C., Little, C.M., Hattermann, T., Jourdain, N.C., Goelzer, H., Nowicki, S., Seroussi, H., Straneo, F., Bracegirdle, T.J., 2020. Cmip5 model selection for ismip6 ice sheet model forcing: Greenland and Antarctica. Cryosphere 14, 855–879. https://doi.org/10.5194/tc-14-855-2020.

Blank, B., Barletta, V., Hu, H., Pappa, F., van der Wal, W., 2021. Effect of lateral and stress-dependent viscosity variations on GIA induced uplift rates in the Amundsen Sea Embayment. Geochem. Geophys. Geosyst. 22, 1–28. https://doi.org/10.1029/2021GC009807.

Blatter, H., 1995. Velocity and stress-fields in grounded glaciers - a simple algorithm for including deviatoric stress gradients. J. Glaciol. 41, 333–344.

Bueler, E., Lingle, C.S., Brown, J., 2007. Fast computation of a viscoelastic deformable Earth model for ice-sheet simulations. Ann. Glaciol. 46, 97–105. https://doi.org/10.3189/172756407782871567.

Chambers, C., Greve, R., Obase, T., Saito, F., Abe-Ouchi, A., 2021. Mass loss of the Antarctic ice sheet until the year 3000 under a sustained late-21st-century climate. J. Glaciol., 1–13. https://doi.org/10.1017/jog.2021.124.

Cornford, S.L., Martin, D.F., Payne, a.J., Ng, E.G., Le Brocq, a.M., Gladstone, R.M., Edwards, T.L., Shannon, S.R., Agosta, C., van den Broeke, M.R., Hellmer, H.H., Krinner, G., Ligtenberg, S.R.M., Timmermann, R., Vaughan, D.G., 2015. Century-scale simulations of the response of the West Antarctic Ice Sheet to a warming climate. Cryosphere 9, 1579–1600. https://doi.org/10.5194/tc-9-1579-2015.

Coulon, V., Bulthuis, K., Whitehouse, P.L., Sun, S., Haubner, K., Zipf, L., Pattyn, F., 2021. Contrasting response of West and East Antarctic ice sheets to Glacial Isostatic Adjustment. J. Geophys. Res., Earth Surf., 1–26. https://doi.org/10.1029/2020jf006003.

DeConto, R.M., Pollard, D., Alley, R.B., Velicogna, I., Gasson, E., Gomez, N., Sadai, S., Condron, A., Gilford, D.M., Ashe, E.L., Kopp, R.E., Li, D., Dutton, A., 2021. The Paris Climate Agreement and future sea-level rise from Antarctica. Nature 593, 83–89. https://doi.org/10.1038/s41586-021-03427-0. arXiv:1011.1669v3.

Dziewonski, A.M., Anderson, D.L., 1981. Preliminary reference Earth model. Phys. Earth Planet. Inter. 25, 297–356. https://doi.org/10.1016/0031-9201(81)90046-7.

Feldmann, J., Levermann, A., 2015. Collapse of the West Antarctic Ice Sheet after local destabilization of the Amundsen Basin. Proc. Natl. Acad. Sci. 112, 14191–14196. https://doi.org/10.1073/pnas.1512482112.

Gillet-Chaulet, F., Durand, G., Gagliardini, O., Mosbeux, C., Mouginot, J., Rémy, F., Ritz, C., 2016. Assimilation of surface velocities acquired between 1996 and 2010 to constrain the form of the basal friction law under Pine Island Glacier. Geophys. Res. Lett. 43, 10,311–10,321. https://doi.org/10.1002/2016GL069937.

Goelzer, H., Coulon, V., Pattyn, F., de Boer, B., van de Wal, R., 2020. Brief communication: on calculating the sea-level contribution in marine ice-sheet models. Cryosphere 14, 833–840. https://doi.org/10.5194/tc-14-833-2020.

Gomez, N., Mitrovica, J.X., Tamisiea, M.E., Clark, P.U., 2010. A new projection of sea level change in response to collapse of marine sectors of the Antarctic Ice Sheet. Geophys. J. Int. 180, 623–634. https://doi.org/10.1111/j.1365-246X.2009.04419.x.

Gomez, N., Pollard, D., Holland, D., 2015. Antarctic Ice-Sheet mass loss. Nat. Commun. 6, 1–8. https://doi.org/10.1038/ncomms9798.

Gomez, N., Latychev, K., Pollard, D., 2018. A coupled ice sheet-sea level model incorporating 3D Earth structure: variations in Antarctica during the last deglacial retreat. J. Climate. JCLI–D–17–0352.1 https://doi.org/10.1175/JCLI-D-17-0352.1.

Hoffman, M.J., Perego, M., Price, S.F., Lipscomb, W.H., Jacobsen, D., Tezaur, I., Salinger, A.G., Tuminaro, R., Zhang, T., 2018. MPAS-Albany Land Ice (MALI): a variable resolution ice sheet model for Earth system modeling using Voronoi grids. Geosci. Model Dev., 1–47. https://doi.org/10.5194/gmd-2018-78.

Hoffman, M.J., Asay-Davis, X., Price, S.F., Fyke, J., Perego, M., 2019. Effect of subshelf melt variability on sea level rise contribution from Thwaites Glacier, Antarctica. J. Geophys. Res., Earth Surf. 124, 2798–2822. https://doi.org/10.1029/2019JF005155.

Ivins, Erik R., James, Thomas S., Wahr, John, Schrama, Ernst J.O., Landerer, Felix W., Simon, Karen M., 2013. Antarctic contribution to sea level rise observed by GRACE with improved GIA correction. J. Geophys. Res., Solid Earth 118 (6). https://doi.org/10.1002/jgrb.50208.

Ivins, E.R., van der Wal, W., Wiens, D.A., Lloyd, A.J., Caron, L., 2021. Antarctic upper mantle rheology. Geol. Soc. Lond. Mem. 56. https://doi.org/10.1144/M56-2020-19.

Joughin, I., Smith, B.E., Medley, B., 2014. Marine ice sheet collapse potentially underway for the Thwaites Glacier basin, West Antarctica. Science 344, 735–738. https://doi.org/10.1126/science.1249055.

Jourdain, N., Asay-Davis, X., Hattermann, T., Straneo, F., Seroussi, H., Little, C., Nowicki, S., 2020. A protocol for calculating basal melt rates in the ISMIP6 Antarctic ice sheet projections. Cryosphere 14, 3111–3134. https://doi.org/10.5194/tc-14-3111-3020.

Kachuck, S.B., 2017. giapy: Glacial Isostatic Adjustment in PYthon (1.0.0) [Source code].

Kachuck, S.B., Cathles, L., 2019. Benchmarked computation of time-domain viscoelastic Love numbers for adiabatic mantles. Geophys. J. Int. https://doi.org/10.1093/gji/ggz276.

Kachuck, S.B., Martin, D.F., Bassis, J.N., Price, S.F., 2020. Rapid viscoelastic deformation slows marine ice sheet instability at Pine Island Glacier. Geophys. Res. Lett. 47, 1–12. https://doi.org/10.1029/2019GL086446.

Konrad, H., Sasgen, I., Pollard, D., Klemann, V., 2015. Potential of the solid-Earth response for limiting long-term West Antarctic Ice Sheet retreat in a warming climate. Earth Planet. Sci. Lett. 432, 254–264. https://doi.org/10.1016/j.epsl.2015.10.008.

Larour, E., Seroussi, H., Adhikari, S., Ivins, E., Caron, L., Morlighem, M., Schlegel, N., 2019. Slowdown in Antarctic mass loss from solid Earth and sea-level feedbacks. Science 364. https://doi.org/10.1126/science.aav7908.

Lau, H.C., Austermann, J., Holtzman, B.K., Havlin, C., Lloyd, A.J., Book, C., Hopper, E., 2021. Frequency dependent mantle viscoelasticity via the complex viscosity: cases from Antarctica. J. Geophys. Res., Solid Earth 126, 1–26. https://doi.org/10.1029/2021JB022622.

Lenaerts, J.T.M., van den Broeke, M.R., van de Berg, W.J., van Meijgaard, E., Kuipers Munneke, P., 2012. A new, high-resolution surface mass balance map of Antarctica (1979-2010) based on regional atmospheric climate modeling. Geophys. Res. Lett. 39, L04501. https://doi.org/10.1029/2011GL050713.

Lloyd, A.J., Wiens, D.A., Zhu, H., Tromp, J., Nyblade, A.A., Aster, R.C., Hansen, S.E., Dalziel, I.W.D., Wilson, T., Ivins, E.R., O'Donnell, J.P., 2020. Seismic structure of the Antarctic upper mantle imaged with adjoint tomography. J. Geophys. Res., Solid Earth 125. https://doi.org/10.1029/2019JB017823.

Martin, D.F., Cornford, S.L., Payne, A.J., 2019. Millennial-scale vulnerability of the Antarctic Ice Sheet to regional ice shelf collapse. Geophys. Res. Lett. 46, 1467–1475. https://doi.org/10.1029/2018GL081229.

Morlighem, M., Rignot, E., Binder, T., Blankenship, D., Drews, R., Eagles, G., Eisen, O., Ferraccioli, F., Forsberg, R., Fretwell, P., Goel, V., Greenbaum, J.S., Gudmundsson, H., Guo, J., Helm, V., Hofstede, C., Howat, I., Humbert, A., Jokat, W., Karlsson, N.B., Lee, W.S., Matsuoka, K., Millan, R., Mouginot, J., Paden, J., Pattyn, F., Roberts, J., Rosier, S., Ruppel, A., Seroussi, H., Smith, E.C., Steinhage, D., Sun, B., den Broeke, M.R., Ommen, T.D., van Wessem, M., Young, D.A., 2020. Deep glacial troughs and stabilizing ridges unveiled beneath the margins of the Antarctic ice sheet. Nat. Geosci. 13, 132–137. https://doi.org/10.1038/s41561-019-0510-8.

Mouginot, J., Rignot, E., Scheuchl, B., 2014. Sustained increase in ice discharge from the Amundsen Sea Embayment, West Antarctica, from 1973 to 2013. Geophys. Res. Lett. 41, 1576–1584. https://doi.org/10.1002/2013GL059069.1.

Mouginot, J., Rignot, E., Scheuchl, B., Millan, R., 2017. Comprehensive annual ice sheet velocity mapping using Landsat-8, Sentinel-1, and RADARSAT-2 data. Remote Sens. 9, 1–20. https://doi.org/10.3390/rs9040364.

Nias, I.J., Cornford, S.L., Payne, A., 2018. New mass-conserving bedrock topography for Pine Island Glacier impacts simulated decadal rates of mass loss. Geophys. Res. Lett. 45, 3173–3181. https://doi.org/10.1002/2017GL076493.

Nield, G.A., Barletta, V.R., Bordoni, A., King, M.A., Whitehouse, P.L., Clarke, P.J., Domack, E., Scambos, T.A., Berthier, E., 2014. Rapid bedrock uplift in the Antarctic Peninsula explained by viscoelastic response to recent ice unloading. Earth Planet. Sci. Lett. 397, 32–41. https://doi.org/10.1016/j.epsl.2014.04.019.

Nield, G.A., Whitehouse, P.L., van der Wal, W., Blank, B., O'Donnell, J.P., Stuart, G.W., 2018. The impact of lateral variations in lithospheric thickness on glacial isostatic adjustment in West Antarctica. Geophys. J. Int. 214, 811–824. https://doi.org/10.1093/gji/ggy158.

Pan, L., Powell, E.M., Latychev, K., Mitrovica, J.X., Creveling, J.R., Gomez, N., Hoggard, M.J., Clark, P.U., 2021. Rapid Postglacial Rebound Amplifies Global Sea Level Rise Following West Antarctic Ice Sheet Collapse, pp. 27–29.

Pattyn, F., 2003. A new three-dimensional higher-order thermomechanical ice sheet model: basic sensitivity, ice stream development, and ice flow across subglacial lakes. J. Geophys. Res. 108, 1–15. https://doi.org/10.1029/2002JB002329.

Perego, M., Price, S., Stadler, G., 2014. Optimal initial conditions for coupling ice sheet models to Earth system models. J. Geophys. Res., Earth Surf. 119, 1–24. https://doi.org/10.1002/2014JF003181.Received.

Pollard, D., Gomez, N., Deconto, R.M., 2017. Variations of the Antarctic ice sheet in a coupled ice sheet-Earth-sea level model: sensitivity to viscoelastic Earth properties. J. Geophys. Res., Earth Surf. 122, 2124–2138. https://doi.org/10.1002/2017JF004371.

Rignot, E., Mouginot, J., Morlighem, M., Seroussi, H., Scheuchl, B., 2014. Widespread, rapid grounding line retreat of Pine Island, Thwaites, Smith, and Kohler glaciers, West Antarctica, from 1992 to 2011. Geophys. Res. Lett. 41, 3502–3509. https://doi.org/10.1002/2014GL060140.

Scambos, T.A., Bell, R.E., Alley, R.B., Anandakrishnan, S., Bromwich, D.H., Brunt, K., Christianson, K., Creyts, T., Das, S.B., DeConto, R., Dutrieux, P., Fricker, H.A., Holland, D., MacGregor, J., Medley, B., Nicolas, J.P., Pollard, D., Siegfried, M.R., Smith, A.M., Steig, E.J., Trusel, L.D., Vaughan, D.G., Yager, P.L., 2017. How much, how fast?: a science review and outlook for research on the instability of Antarctica's Thwaites Glacier in the 21st century. Glob. Planet. Change 153, 16–34. https://doi.org/10.1016/j.gloplacha.2017.04.008.

Schoof, C., 2007. Ice sheet grounding line dynamics: steady states, stability, and hysteresis. J. Geophys. Res. 112, 1–19. https://doi.org/10.1029/2006JF000664.

Seroussi, H., Nakayama, Y., Larour, E., Menemenlis, D., Morlighem, M., Rignot, E., Khazendar, A., 2017. Continued retreat of Thwaites Glacier, West Antarctica, controlled by bed topography and ocean circulation. Geophys. Res. Lett., 1–9. https://doi.org/10.1002/2017GL072910.

Seroussi, H., Nowicki, S., Payne, A.J., Goelzer, H., Lipscomb, W.H., Abe-Ouchi, A., Agosta, C., Albrecht, T., Asay-Davis, X., Barthel, A., Calov, R., Cullather, R., Dumas, C., Galton-Fenzi, B.K., Gladstone, R., Golledge, N.R., Gregory, J.M., Greve, R., Hattermann, T., Hoffman, M.J., Humbert, A., Huybrechts, P., Jourdain, N.C., Kleiner, T., Larour, E., Leguy, G.R., Lowry, D.P., Little, C.M., Morlighem, M., Pattyn, F., Pelle, T., Price, S.F., Quiquet, A., Reese, R., Schlegel, N.J., Shepherd, A., Simon, E., Smith, R.S., Straneo, F., Sun, S., Trusel, L.D., Van Breedam, J., van de Wal, R.S.W., Winkelmann, R., Zhao, C., Zhang, T., Zwinger, T., 2020. ISMIP6 Antarctica: a multi-model ensemble of the Antarctic ice sheet evolution over the 21st century. Cryosphere 14, 3033–3070. https://doi.org/10.5194/tc-14-3033-2020.

Shapiro, N.M., Ritzwoller, M.H., 2004. Inferring surface heat flux distributions guided by a global seismic model: particular application to Antarctica. Earth Planet. Sci. Lett. 223, 213–224. https://doi.org/10.1016/j.epsl.2004.04.011.

Simms, A.R., Ivins, E.R., DeWitt, R., Kouremenos, P., Simkins, L.M., 2012. Timing of the most recent Neoglacial advance and retreat in the South Shetland Islands, Antarctic Peninsula: insights from raised beaches and Holocene uplift rates. Quat. Sci. Rev. 47, 41–55. https://doi.org/10.1016/j.quascirev.2012.05.013.

Tezaur, I.K., Perego, M., Salinger, A.G., Tuminaro, R.S., Price, S., 2015. Albany/FELIX: a parallel, scalable and robust, finite element, first-order Stokes approximation ice sheet solver built for advanced analysis. Geosci. Model Dev. 8, 1–24. https://doi.org/10.5194/gmd-8-1-2015.

van den Broeke, M.R., 2019. RACMO2.3p1 annual surface mass balance Antarctica (1979-2014). https://doi.org/10.1594/PANGAEA.896940.

Waibel, M.S., Hulbe, C.L., Jackson, C.S., Martin, D.F., 2018. Rate of mass loss across the instability threshold for Thwaites Glacier determines rate of mass loss for entire basin. Geophys. Res. Lett. 45, 809–816. https://doi.org/10.1002/2017GL076470.

Wan, J.X.W., Gomez, N., Latychev, K., Han, H.K., 2021. Resolving GIA in response to modern and future ice loss at marine grounding lines in West Antarctica. Cryosphere Discuss., 1–32. https://doi.org/10.5194/tc-2021-232.

Whitehouse, P.L., Gomez, N., King, M.A., Wiens, D.A., 2019. Solid Earth change and the evolution of the Antarctic Ice Sheet. Nat. Commun. 10, 503. https://doi.org/10.1038/s41467-018-08068-y.

Wu, Patrick, Peltier, W.R., 1982. Viscous gravitational relaxation. Geophys. J. Int. 70 (2), 435–485. https://doi.org/10.1111/j.1365-246X.1982.tb04976.x.

Yu, H., Rignot, E., Seroussi, H., Morlighem, M., 2018. Retreat of Thwaites Glacier, West Antarctica, over the next 100 years using various ice flow models, ice shelf melt scenarios and basal friction laws. Cryosphere 12, 3861–3876. https://doi.org/10.5194/tc-12-3861-2018.

Yu, H., Rignot, E., Seroussi, H., Morlighem, M., Choi, Y., 2019. Impact of iceberg calving on the retreat of Thwaites Glacier, West Antarctica over the next century with different calving laws and ocean thermal forcing. Geophys. Res. Lett. 46, 14539–14547. https://doi.org/10.1029/2019GL084066.